# CHAPTER II

# GROWTH AND CHARACTERISATION TECHNIQUES

The experimental details are explained in this chapter. It consists of two main parts: molecular beam epitaxy and characterization techniques which include reflection high-energy electron diffraction, atomic force microscopy, photoluminescence, transmission electron microscopy, and X-ray diffraction techniques.

## 2.1 Molecular Beam Epitaxy (MBE)

Molecular beam epitaxy is a precise and versatile crystal growth technique. In MBE, a perfect crystal is formed by the deposition of one or more pure materials onto a single crystal wafer under ultra-high vacuum. In solid-source MBE, different material source cells in separate crucibles are heated with separate heaters. They are evaporated and condensed on a wafer, where they react with each other, forming a crystal. A special advantage of MBE, compared to other growth techniques, is that a computer-controlled shutter in front of each cell allows precise control over layer thickness and composition. The mechanical shutters in front of the sources can be closed and opened in less than 1 second. The temperatures of the sources can be accurately controlled. The composition of the epilayer and its doping level depend on the relative arrival rates of the constituent elements and dopants, which in turn depend on the evaporation rates of the appropriate sources. This makes it possible for MBE to grow sub-atomic layers.

### 2.1.1 MBE System Overview

A typical MBE machine consists of four chambers: load chamber, introduction chamber, transfer chamber, and growth chamber. These chambers are separated by isolated gate valves and the samples are transferred from one chamber to another by a magnetic arm. The introduction and the growth chambers have heaters for a heat treatment process (preheat) of the substrate. Ultra-high vacuum condition is obtained

หอสมุดกลาง ศูนย์วิทยทรัพยากร
จุฬาลงกรณ์มหาวิทยาลัย


via a pumping system which consists of sorption pump, ion pump, and titanium sublimation pump.

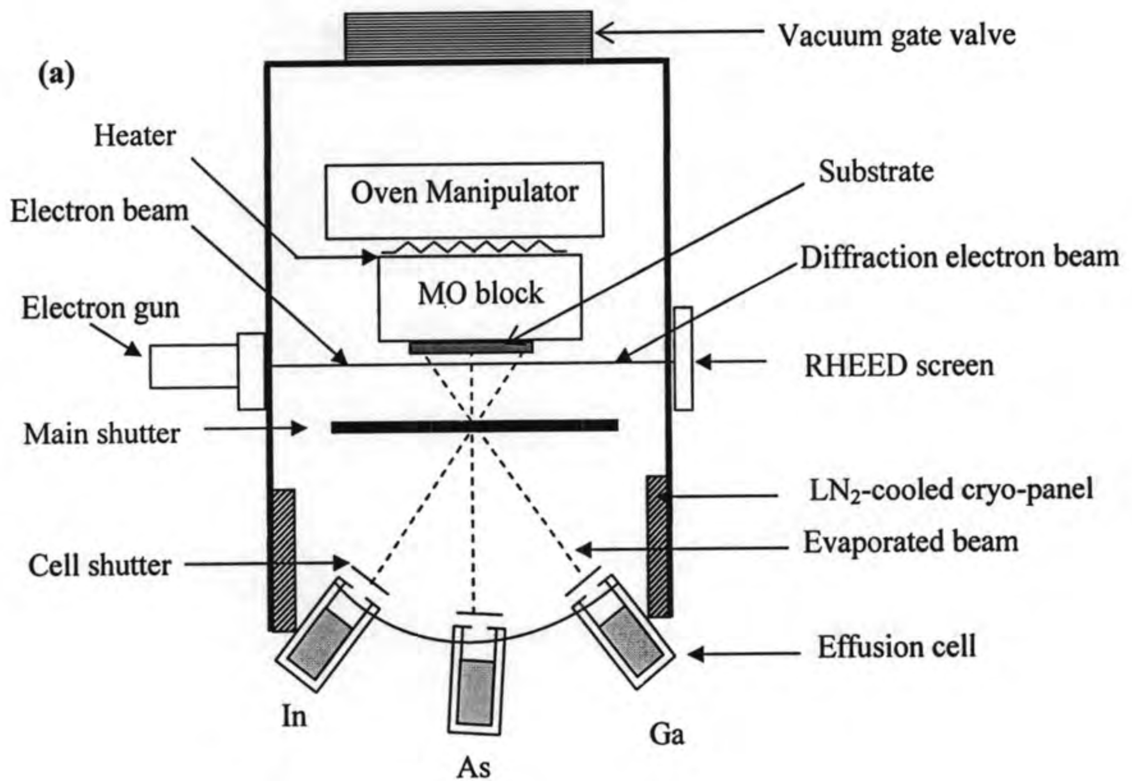


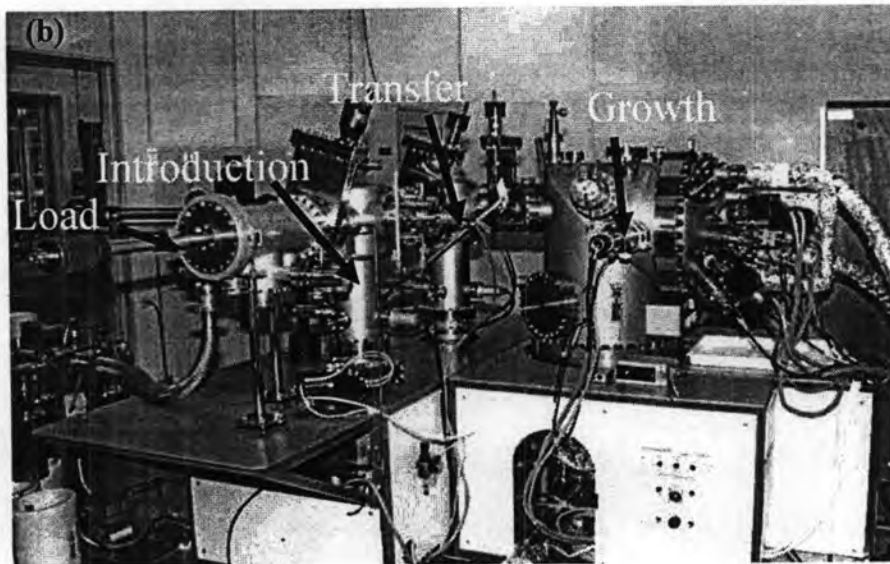


Figure 2.1 (a) Schematic diagram of the growth chamber and (b) a photograph of RIBER 32P MBE system.

The schematic drawing of a typical MBE growth chamber is shown in Fig. 2.1(a). Inside the growth chamber are material source cells, substrate heater, monitoring equipment, and a pumping system. The solid-source materials are separately contained in different effusion cells. During growth, the chamber wall and the effusion cells are cooled with liquid nitrogen ($LN_2$) to prevent contaminations as a result of outgassing from heated parts. Two types of monitoring equipment are used: mass spectroscopy and reflection high-energy electron diffraction (RHEED). The mass spectroscopy is used for particle analysis while RHEED is used as a tool to observe surface crystalinity. There are two ionization gauges which measure the beam flux and background pressure (BP). One of the ionization gauges measuring for BEP is located at the same level of manipulator behind the substrate heater and the other guage is situated in front of the ion pump for measuring the BP. The temperature is measured by W-Re thermocouples and controlled by computer via a controller card (EUROTHERM). In order to get a uniform flux profile on the substrate's surface, the substrate is continuously rotated by a motor during epitaxy.

In all experiments, samples are grown on semi-insulating (001)-GaAs substrates in a solid-source MBE system (RIBER 32P) shown in Fig. 2.1(b). The substrate is attached to a molybdenum block (MO in the figure). Prior to crystal growth, contaminations are removed from the substrate surface by a 3-hour pre-heat process in the introduction chamber before being transferred to the growth chamber. The pre-heat process is done when the pressure in the introduction chamber is $1\times10^{-8}$ Torr or lower. The temperature profile of the pre-heat process is shown in Fig. 2.2.

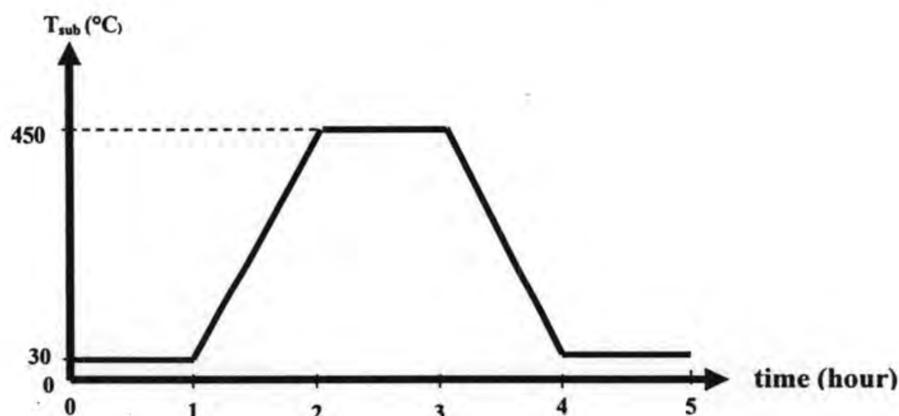


Figure 2.2 Temperature profile of the pre-heat process.

In the pre-heat process, the sample is heated by increasing the substrate temperature ($T_{sub}$) from 30°C to 450°C at a rate of 7°C/min. This ramp up takes 1 hour. During the ramp up, the contaminations from the substrate surface are removed and purged; the pressure inside the introduction chamber thus increases. When the $T_{sub}$ reaches 450°C, it is held for 1 hour. Then, the $T_{sub}$ is ramped down from 450°C to 30°C. The pre-heat process thus takes 3 hours in total and all samples are subject to this process without exception.

After the pre-heat process, the sample is transferred to the growth chamber and a de-gas process is carried out. In the de-gas process, the temperature of each cell is increased from the standby temperature ($T_{std}$) to the required temperature in order to remove the contaminations from each cell. The temperature profile of the de-gas process for the temperature ramping up of Ga and In cells are shown Fig. 2.3 and As cells and substrate are shown in Fig. 2.4.

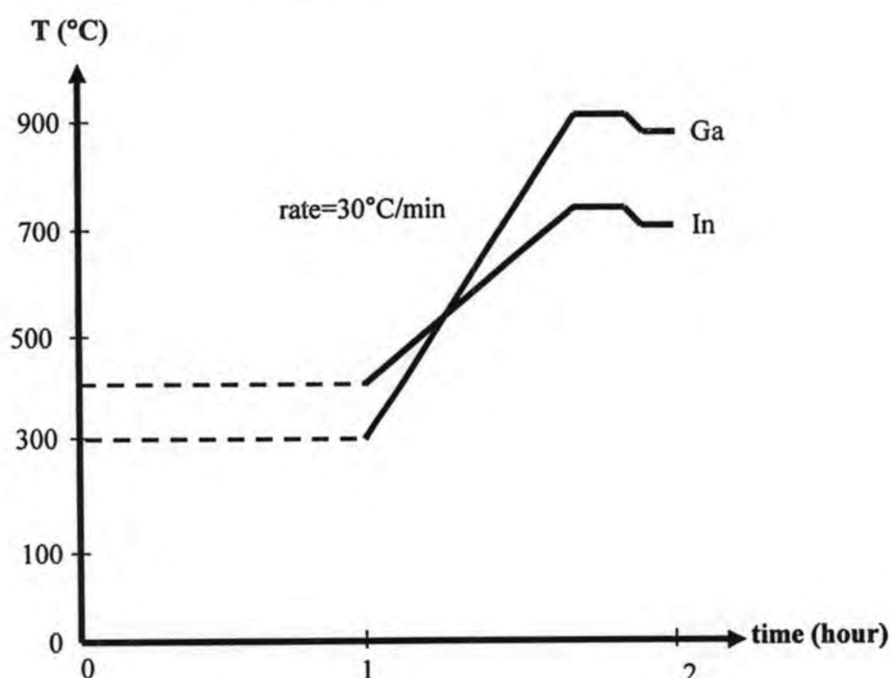


Figure 2.3 Temperature profile of Ga and In cells. The cells are closed in the dotted line range and opened in solid line range during respective temperature ranges.

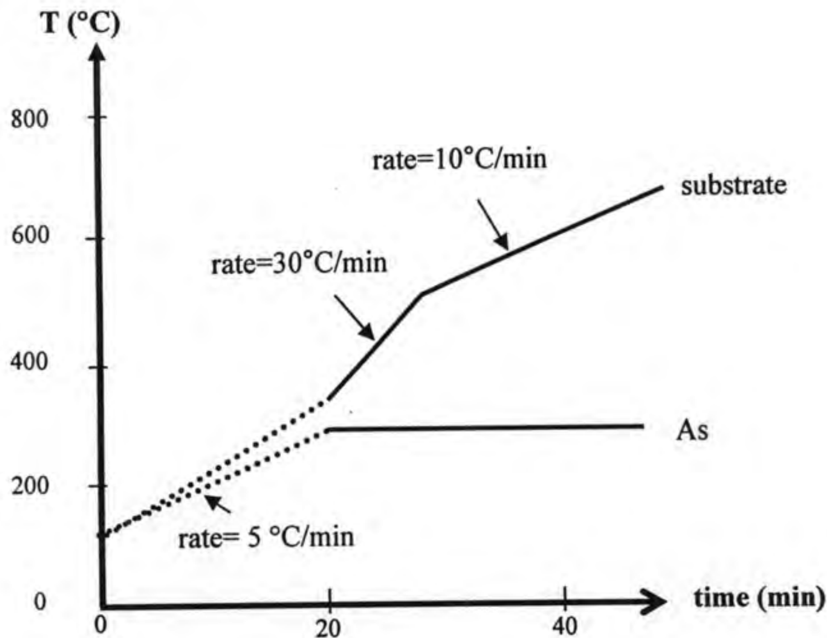


Figure 2.4 Temperature profile As cell and substrate. The cells are closed in the dotted line range and opened in solid line range during respective temperature ranges.

In Fig 2.3, the temperatures of Ga and In cells are increased from their $T_{std}$ to the required temperatures at the same rate of 30°C/min. After ramping up the temperatures of the cells, the pressure of each cell is measured by opening the corresponding cell. Typical BEP of In, Ga and As cells are $\sim 10^{-8}$, $\sim 10^{-7}$ and $\sim 10^{-6}$ Torr respectively. The de-gas process of As cell is done last because the BEP of As cell is significantly higher than other cells. In the de-gas process of As cell, the temperatures of As cell and substrate are ramped up at the same time from the $T_{std}$ 100°C to 300°C at the same rate of 5°C/min in order to suppress the As atoms outgassing from the substrate surface. When the $T_{sub}$ is higher than 300°C, outgassing As atoms from the substrate results in surface roughness. Between 300°C to 500°C, the rate is increased to 30°C/min. Between 500°C to 650°C, the rate is 10°C/min.

After the de-gas process which prepares the cells for growth, the substrate has to go to the de-ox process in order to prepare the surface for subsequent epilayer growth. The de-ox process and RHEED pattern for the substrate when the temperature increases in this process is shown in Fig. 2.5(a). When $T_{sub}$ is around 580°C, a spotty pattern such as the photo shown in Fig. 2.5(b) starts to occur because

the native oxide comes out of the GaAs surface. To ensure complete oxide removal and thus a clean GaAs surface, the temperature is kept at slightly above the de-ox temperature. Usually, if $T_{deox}$=580°C, the temperature would be kept at 590°C until the CO peak is almost flat which can be observed from the quadrupole mass spectroscopy system. Otherwise, the substrate surface will be resulted in rough morphology after being the GaAs buffer layer growth according to the experimental observations.

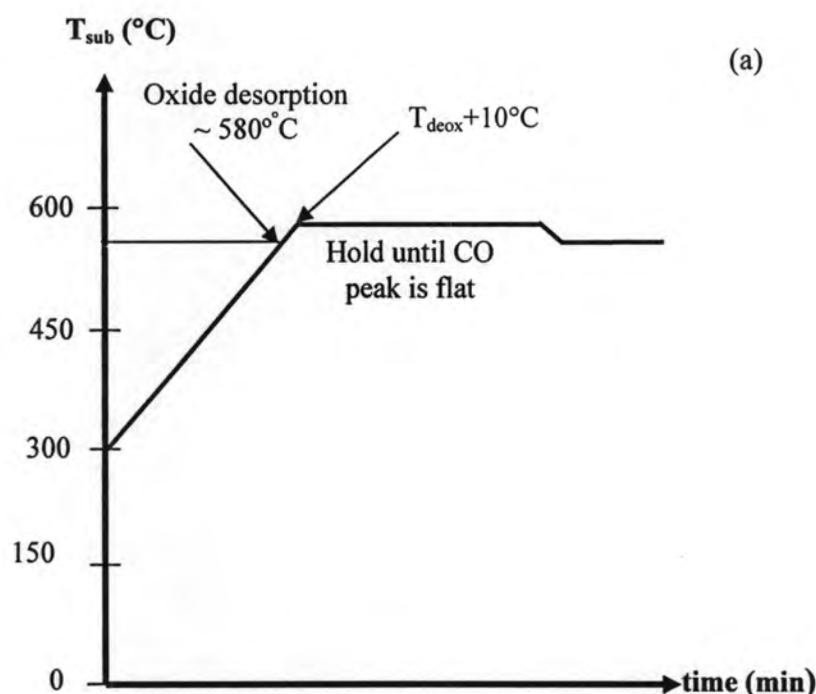


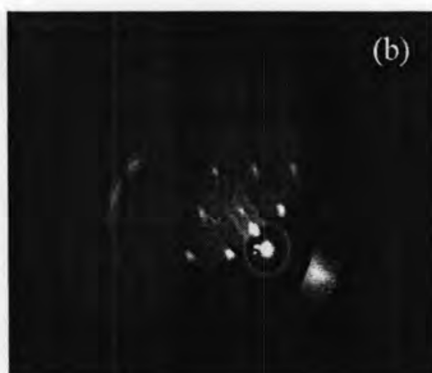


Figure 2.5 (a) Temperature profile for the oxide desorption process and RHEED pattern when the temperature increases and (b) photo taken from the viewport showing RHEED spotty pattern at de-ox temperature (580°C).

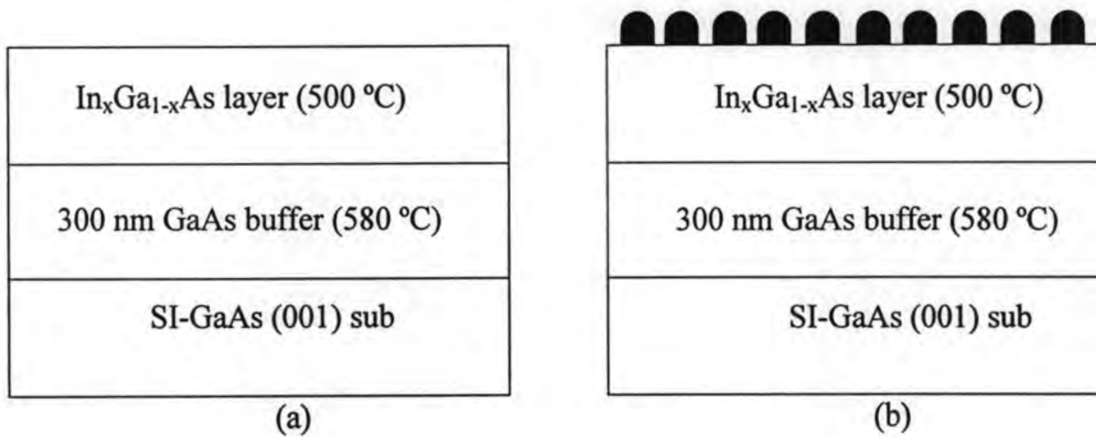


Figure 2.6 Cross-section of MBE samples grown in order to study the surface morphology of (a) strain relaxed InGaAs layer and (b) QDs formed on strain relaxed layer.

After oxide desorption, a 300-nm GaAs buffer layer is grown to flatten the surface at a rate of 0.34 ML/s at 580°C for all samples. The $T_{sub}$ is then reduced to 500°C in order to grow $In_xGa_{1-x}As$ (x=0.10, 0.13, 0.15) strained layers. For the studies of strain relaxation of InGaAs layers, a short growth interruption (GI) is introduced before the substrate temperature is rapidly ramped down to 100°C. The schematic cross-section of the wafer subject to such growth procedure is shown in Fig. 2.6(a). For the study of QDs formation on the strain relaxed layers, InAs QDs are grown on the InGaAs layer at 500°C and the schematic cross-section of a typical sample is shown in Fig. 2.6(b).

During growth, the growth rate of InAs for the study of strained relaxed InGaAs layer is 0.06 ML/s and QDs is 0.01 ML/s. The BEP of $As_4$ is fixed at $3.5\times10^{-6}$ Torr. The structure shown in Fig. 2.6(b) is suitable for surface studies by ex-situ AFM. For optical properties, however, the sample needs to be capped with a thin layer (100 nm) of GaAs.

### 2.1.2 In-Situ Characterisation Tools

Two important in-situ characterisation tools are mass spectroscopy and RHEED. Mass spectroscopy is used to investigate the chemical constitutes inside the growth

chamber. RHEED is used to calibrate the growth rates and to indicate the 2D to 3D growth mode transition point.

#### 2.1.2.1 Mass Spectroscopy (An introduction to Mass Spectroscopy, Ashcroft)

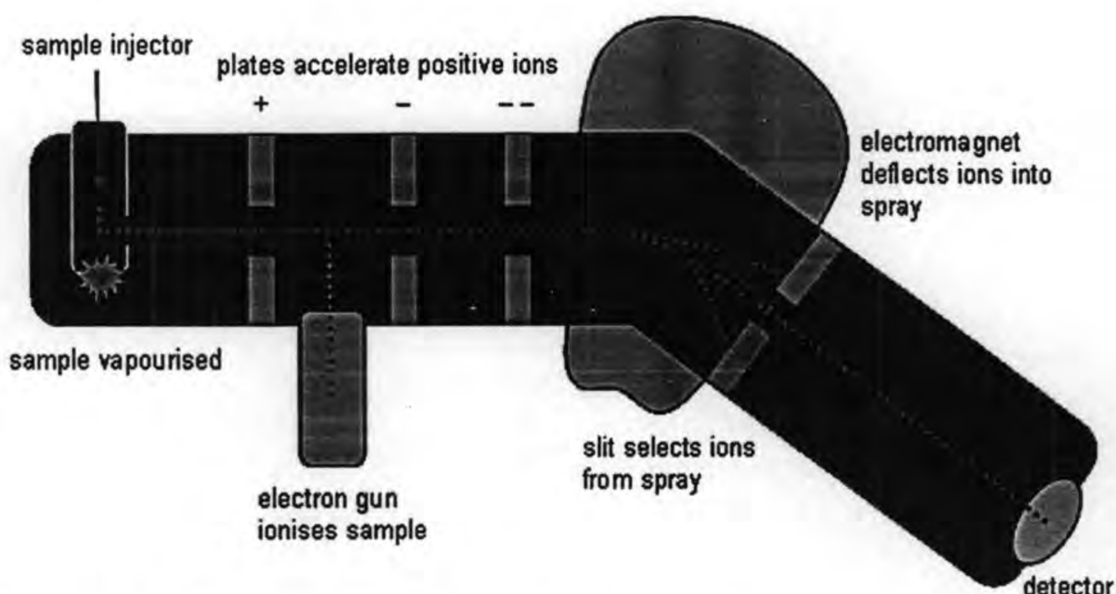


Figure 2.7 A schematic diagram of mass spectrometer (http://www.stev.gb.com/science/spectroscopy.html).

Mass spectrometry is an analytical technique used to measure the mass-to-charge (m/z) ratio of ions. The composition of a sample can be determined from the mass spectrum representing the masses of sample components. A typical mass spectrometer comprises three parts: an ion source, a mass analyzer, and a detector system. A schematic diagram of mass spectrometer is shown in Fig. 2.7. The sample has to be introduced into the ionisation source of the instrument. Once inside the ionisation source, the sample molecules are ionised, because ions are easier to manipulate than neutral molecules. These ions are extracted into the analyser region of the mass spectrometer where they are separated according to their mass-to-charge ratios. The separated ions are detected and this signal sent to a data system where the m/z ratios are stored together with their relative abundance for presentation in the format of a m/z spectrum.

The analyser and detector of the mass spectrometer, and often the ionisation source too, are maintained under high vacuum to give the ions a reasonable chance of travelling from one end of the instrument to the other without any hindrance from air molecules. The entire operation of the mass spectrometer, and often the

sample introduction process also, is under complete data system control on modern mass spectrometers.

In all experiments, masses of the particles such as hydrogen, helium, argon, water, oxygen, carbon dioxide and carbon monoxide are checked by mass spectrometer. Specifically, the complete removal of native oxide from the substrate surface is investigated by mass spectrometer. In the de-ox process, when the signal of 28 peak (carbon monoxide) is almost flat, further growth process is continued.

#### 2.1.2.2 Reflection High-Energy Electron Diffraction (RHEED)

Reflection high-energy electron diffraction gives information of the dynamics of MBE growth (Sakamoto et al., 1986; Larsen et al., 1987). The RHEED system is a main tool for observing and measuring important parameters such as growth rates. Direct information such as surface quality and indirect information such as substrate temperature can also be known from the RHEED (Alexeev et al., 1996; Farrel and Plastrøm, 1990). It is also a useful technique for the study of kinetics process of MBE growth (Venkatasubraminan et al., 1996; Franke et al., 1998). Alloy composition can also be determined from RHEED observation (Sakamoto, 1988).

The schematic diagram of the RHEED geometry showing an incident electron beam at a small angle θ (1-3°) to the surface plane is shown in Fig. 2.8. After the electron beam incident on the substrate surface, it is diffracted, giving rise to the reconstructed diffraction pattern that appears on the fluorescent screen. The kind of reconstruction depends on the material, the surface orientation and the surface termination (Biasiol and Sobra, 2001). There are two kinds of diffraction patterns: transmission reflection diffraction and the true reflection diffraction. The former results in spotty features while the latter provides streaky features. For the diffraction on smooth surfaces, elongated streaks occur. Spotty features usually occur for the diffraction on rough surfaces. Since the penetration of the electron beam is restricted to the uppermost atomic layer (Marten and Meyer-Ehmsen, 1985), the surface layer is represented in reciprocal lattice space rods which perpendicularly direct to the real surface and reflect the surface configuration in atomic scale (Herman and Sitter, 1989).

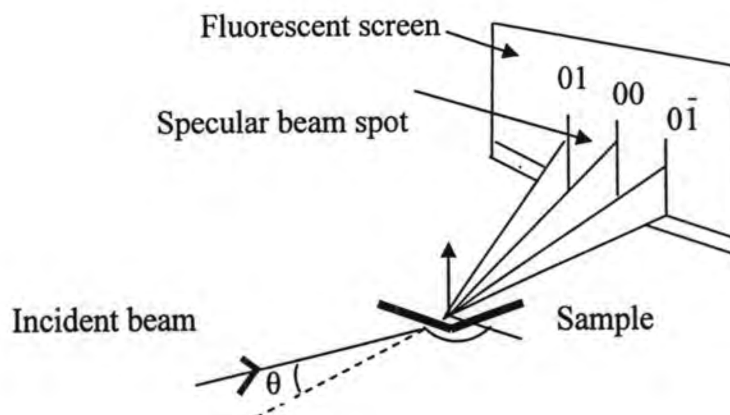


Figure 2.8 Schematic representation of RHEED geometry showing the incident electron beam at an angle θ to the surface plane (Herman and Sitter, 1989).

In order to get desired compositions of In, Ga and As atoms in InGaAs layers under study, the growth rates of InAs and GaAs need to be determined and calibrated. In this work, the change of the RHEED pattern with temperature is used for temperature calibration (i.e. to define the growth temperature of InAs QDs) while the RHEED intensity oscillation is used for growth rate calibration. The details of these two steps are given as follows:

#### 2.1.2.2.1 Temperature calibration

The purpose of temperature calibration is to define the real surface temperature of the substrate because the temperature read from the thermocouple is not the substrate's temperature. Therefore, the reconstruction of RHEED pattern transition as a function of $T_{sub}$ is used to calibrate the absolute temperature of the substrate surface. For the GaAs (001) surface, As-stabilized reconstruction pattern during the growth of GaAs under an excess of As is defined as c(2×4) pattern, while Ga-stabilized is defined as (4×2) or c(4×4) pattern (McCoy et al., 1998). After growing the GaAs buffer layer at the oxide desorption temperature ($T_{deox}$ 580°C), a pattern transition procedure must be followed for accurate temperature determination. The $T_{sub}$ for the formation of QDs is defined as 500°C (Farrell and Palmstrøm, 1990). The temperature

profile and associated RHEED images during temperature calibration is shown in Fig. 2.9.

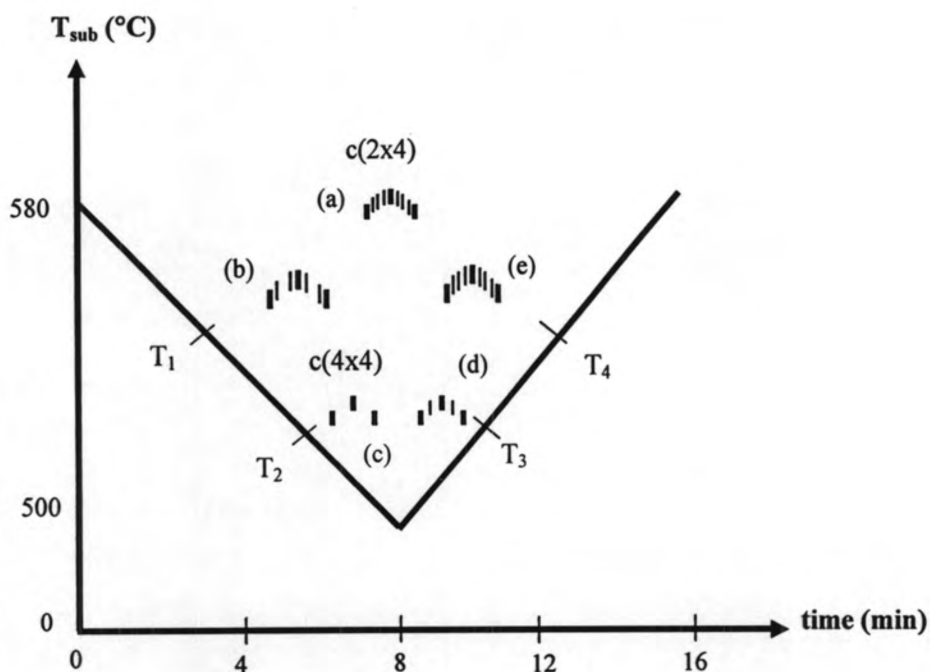


Figure 2.9 Temperature profile and associated RHEED images during temperature calibration.

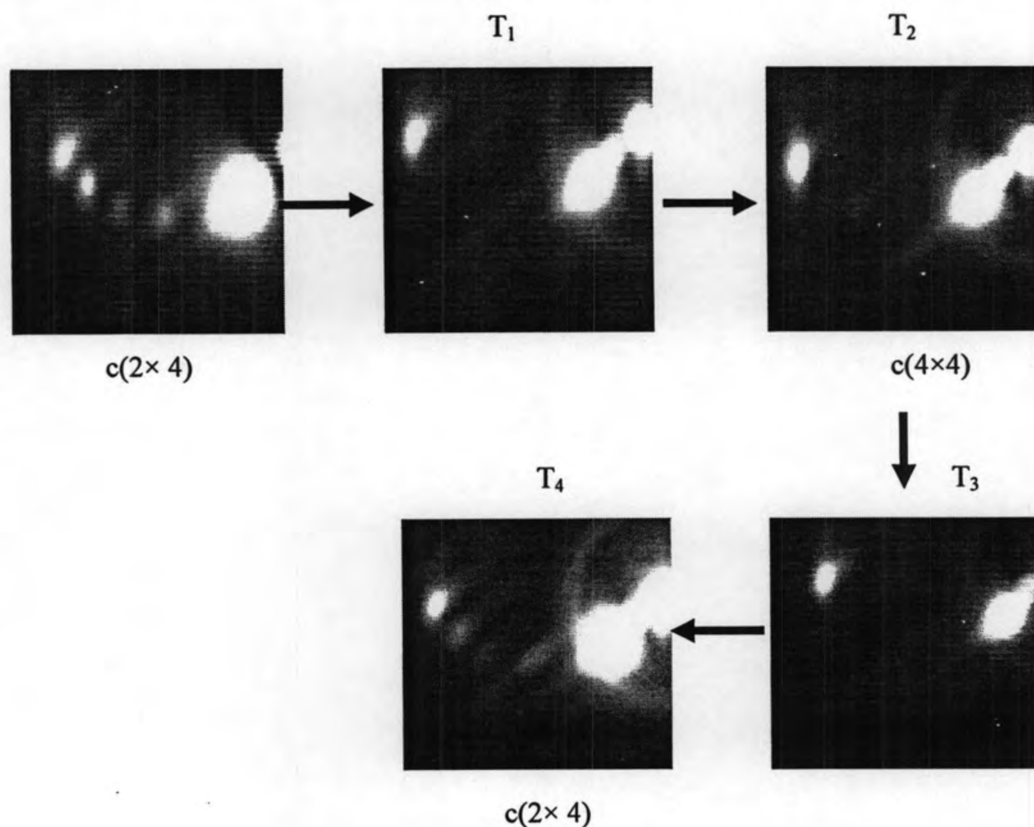


Figure 2.10 Photos of the RHEED patterns taken from the viewport showing (2×4)-(4×4) reconstruction pattern of GaAs surface.

In Fig.2.9, the $T_{sub}$ is decreased at a rate of 10°C/min from 580°C until the RHEED pattern changes from c(2×4) (point a) to the pattern (point b). The temperature at the point b is designated as $T_1$. Then, $T_{sub}$ is further decreased from $T_1$ to c(4×4) pattern (point c). The temperature at the point c is designated as $T_2$. After that, $T_{sub}$ is increased again from the $T_2$ to a pattern (point d). The temperature at the point d is designated as $T_3$. Again, $T_{sub}$ is further increased until c(2×4) pattern (point e). The temperature at the point e is designated as $T_4$. The real surface temperature of the substrate is the average temperature of $T_1$, $T_2$, $T_3$ and $T_4$ which is defined as the real surface temperature of substrate, 500°C. The photos of RHEED reconstruction pattern of GaAs surface showing c(2×4)-c(4×4) pattern is shown in Fig. 2.10. In this figure, the changing of RHEED patterns is related to changes in GaAs surface roughness.

#### 2.1.2.2.2 Growth rate calibration

The growth rates of GaAs ($R_{GaAs}$) and InAs ($R_{InAs}$) are determined from specular beam of RHEED intensity oscillations. The purpose of growth rate calibration is in order to get the desired thicknesses and composition of required layers.

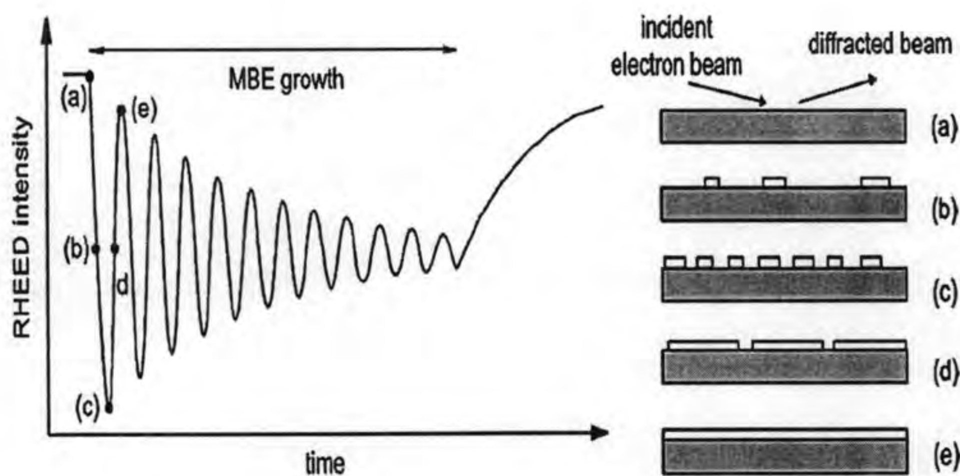


Figure 2.11 Different stages of layer-by-layer growth by nucleation of 2D islands and the corresponding intensity of the zero-order diffracted RHEED beam (Franchi et al., 2003).

A typical RHEED intensity oscillation with schematic diagram of the interpretation of corresponding to GaAs with different coverages is shown in Fig. 2.11 (Franchi et al., 2003). After starting the growth of GaAs (Fig. 2.11a), 2D layer-by-layer islands or surface step features on the growing surface increase until they reach maximum value (Fig. 2.11c). Due to higher surface density of steps, the diffracted beam intensity oscillation shows a minimum in this growth stage. As the growth proceeds, 2D islands tend to coalescence and the density of atomic surface steps reduces (Fig. 2.11d). Correspondingly, the diffracted beam intensity oscillation increases more. Finally, it reaches a maximum value when the GaAs coverage is 1ML (Fig. 2.11e). Therefore, the period of RHEED intensity oscillation corresponds to the growth of 1 ML.

For $R_{GaAs}$ calibration, GaAs buffer layers are grown until c(2×4) RHEED reconstruction pattern is clearly seen. Then, the Ga shutter is closed and the motor is stopped at a position where the specular beam can be clearly seen. A stop watch is used to count the number of RHEED intensity oscillations, typically 10 oscillations. The growth rate is calculated by dividing the number of ML grown (the number of oscillations) by the time. This process is repeated at different Ga temperatures and the results are shown in Fig. 2.12(a).

For $R_{InAs}$ calibration, InAs QDs is grown on GaAs buffer layer at $T_{sub}$ = 500°C. The RHEED pattern transition from a streaky (2D) to a spotty (3D) pattern indicating the formation of InAs QDs on GaAs is defined as 1.7 ML (Shchukin and Bimberg, 1999). The growth rate of InAs is defined as the ratio of 1.7 ML to the time taken from the opening of In shutter to when the 2D-to-3D pattern transition occurs. InAs QDs is grown at different In temperatures and the growth rates at different temperatures are shown in Fig. 2.12(b).

The growth rate of InGaAs can also be determined from RHEED intensity oscillation by adding Ga during the InAs deposition or by simply adding the growth rates of InAs and GaAs: $R_{InGaAs} = R_{GaAs} + R_{InAs}$. From the growth rates of GaAs and InAs, the alloy composition can simply be determined by the relative group III fluxes reaching the surface since the sticking coefficients of group III elements are unity. The In composition in $In_xGa_{1-x}As$ can be determined from:

$$x = \frac{R_{InAs}}{R_{InAs} + R_{GaAs}} \tag{2.1}$$

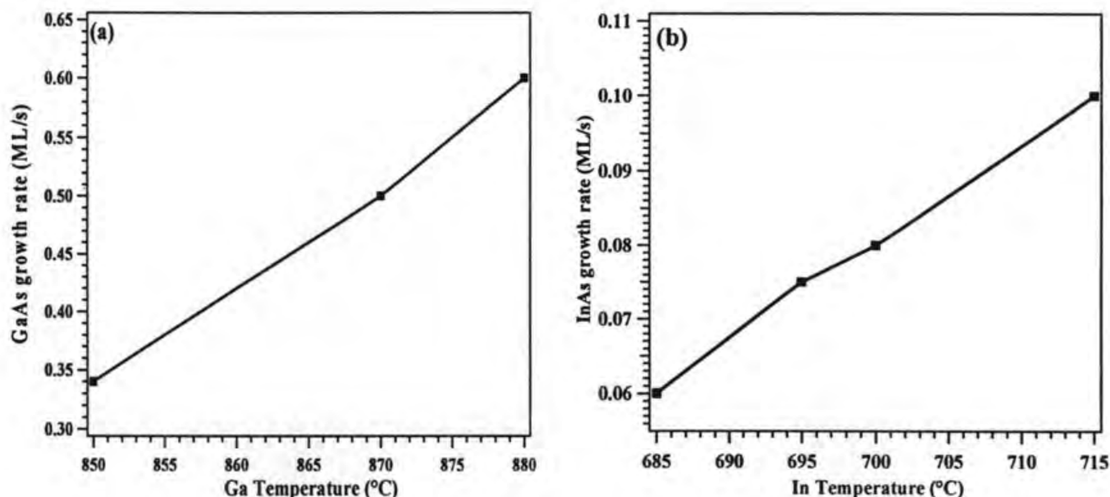


Figure 2.12 Dependence of growth rates of (a) GaAs on the Ga temperature and (b) InAs on the In temperature. BEP of $As_4$ source is kept at $3.5\times10^{-6}$ Torr and the BP during growth is ~ $10^{-7}$ Torr.

## 2.2 Atomic Force Microscopy (AFM)

Atomic force microscopy is a powerful microscope for the observation of matter at nanoscale. The AFM provides a 3D surface profile and can analyse heights at the sub-nm level. A schematic diagram of AFM is shown in Fig. 2.13. The AFM machine consists of a cantilever, a tip, laser beam, photo diode (detector), and feedback electronics. The van der Waals force between the tip and the sample causes deflection of the cantilever. The deflection can be measured using a laser beam reflected off the back of the cantilever onto the photodetectors array. The feedback mechanism is responsible for adjusting the tip-to-sample distance in order to avoid the physical contact between them during scanning.

The AFM can operate in three modes: contact mode, non-contact mode, and dynamic contact mode or tapping mode. In the contact mode operation, a constant deflection is maintained to keep the force constant during the scanning. In the non-contact mode, the cantilever is oscillated externally in order to avoid tip-sample contact. In the dynamic contact or tapping mode, the cantilever is oscillated so that the tip comes into contact with the sample in each period of scanning. Frequency and amplitude modulations provide surface information in the non-contact and the dynamic contact modes. The change in oscillation frequency provides information of

the sample while the change in amplitude provides topographic information of the sample.

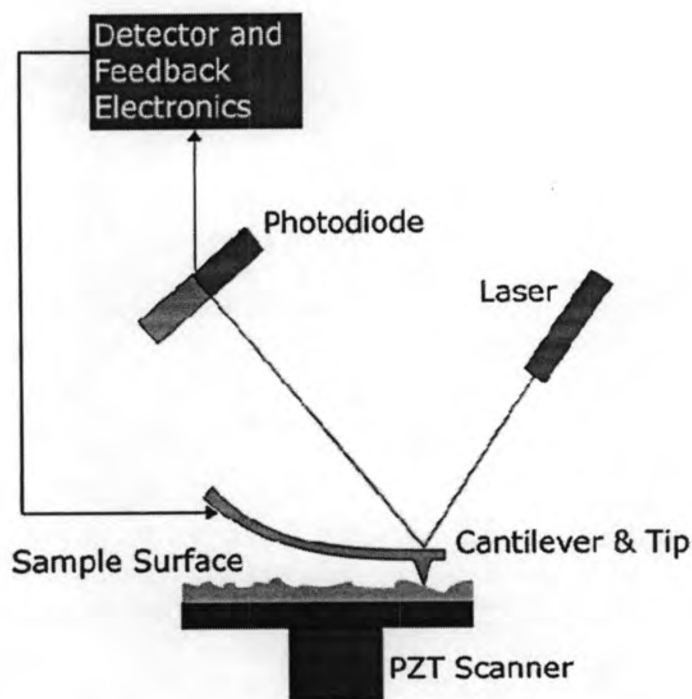


Figure 2.13 Schematic drawing of AFM experimental set up (Allen Timothy Chang, UC Berkeley, 2002).

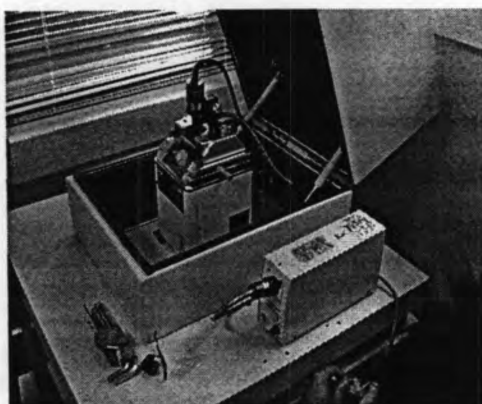

Figure 2.14 Photo of the AFM machine (SPA-400 SPM unit).

The purpose of AFM scanning is in order to study the surface morphology of samples. The size distribution of QDs from AFM analysis is used to determine the size homogeneity of QDs. All of the following AFM imaging is done using Seiko

Instrument's SPA-400 SPM unit shown in Fig. 2.14 via the dynamic force microscope (DFM) scanning operation or the tapping mode. It can scan the area from several hundreds nm to μm (25 μm). The vertical resolution is better than 0.2 nm.

## 2.3 Photoluminescence (PL)

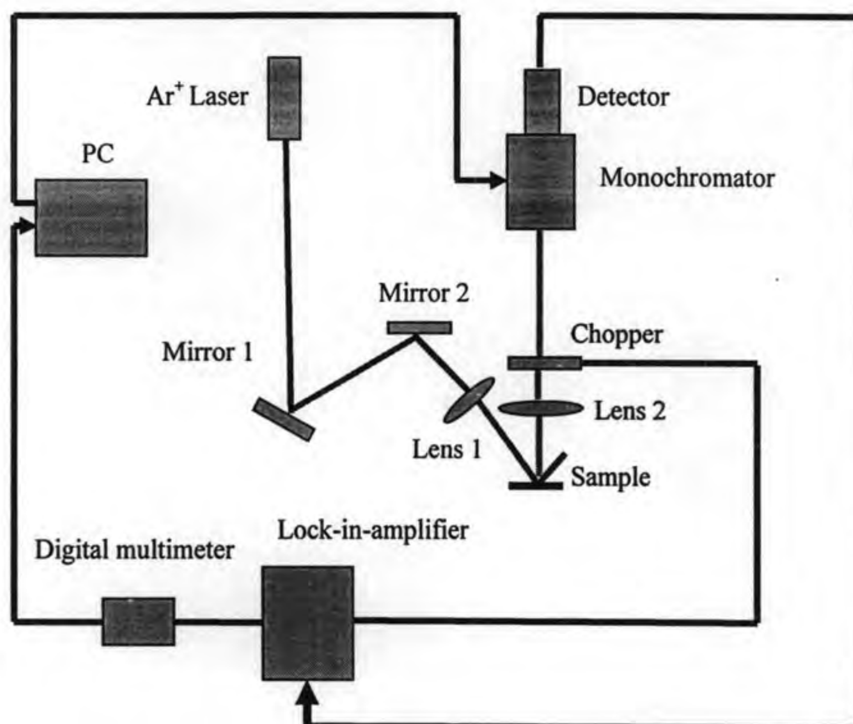


Figure 2.15 Schematic diagram of PL experimental set up.

Luminescence is a property of light emission of a semiconductor when excited with some form of energy. When the semiconductor is excited by photons of appropriate energy, electron-hole pairs are generated and recombined. The resulting radiation from the recombination of carriers is called photoluminescence (PL). PL spectroscopy is a useful tool for sample characterisation which includes the determination of many properties of semiconductor materials such as intrinsic electronic properties, crystal perfection (Hummel et al., 1992; Swaminathan et al., 1985; Kubo et al., 1985) and impurity incorporation (Goetz et al.,1983; Louati et al., 1987).

The schematic diagram of the PL experimental set up is shown in Fig. 2.15. The sample is excited by a 514 nm $Ar^+$ ion laser which corresponds to energy of

2.412 eV. This energy is high enough for pumping electrons across the GaAs energy band gap ($E_g$= 1.424 eV at 300 K). The incoming laser beam, which is successively passed through mirrors 1 and 2 in this figure, is collected by a 15 cm focal length lens (lens 1) and then incidents on the sample. The outgoing light signal (PL) from the sample is collected by a 13.5 nm focal length lens (lens 2) and then passed through a chopper. The dispersed light is then passed through a monochromator (SPE 1000M) and a photodetector. A lock-in amplifier (EG&G 5101) is used to enhance the output signal. The output from the InGaAs photodetector (HAMAMATSU G-7754-01) is fed to the lock-in amplifier. The spectral response range is 1.2 to 2.4 μm. The amplified output is subsequently read by a digital multimeter.

## 2.4 Transmission Electron Microscopy (TEM)

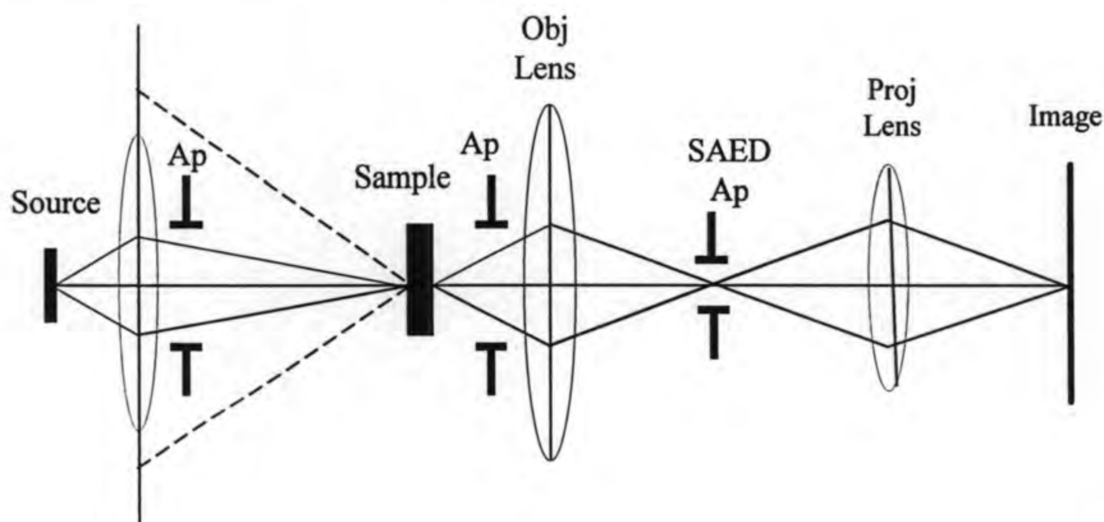


Figure 2.16 Ray diagram of a conventional transmission electron microscopy (Poole and Owens, 2003). The selected area electron diffraction (SAED), aperture (Ap), the sample, the objective (Obj) and projector (Proj) are indicated.

Transmission electron microscopy is one of the imaging techniques of electron microscopy. A ray diagram of a typical TEM is shown in Fig. 2.16 (Poole and Owens, 2003). Materials must be thin enough to allow electrons to transmit through. Emitted electron beams from the source are incident on the sample,

หอสมุดกลาง ศูนย์วิทยทรัพยากร
จุฬาลงกรณ์มหาวิทยาลัย


diffracted by the atoms, and then transmitted to the other side of the sample and are focused by an objective lens and amplified by magnifying (projector) lens. After that, the amplified electron beams hit a fluorescence screen and the information about the inner structure of the sample is displayed in real time on a monitor. By using selected area electron diffraction aperture (SAED) located between the objective and projector lenses, bright- and dark-field images can be selected.

In the bright-field image, the aperture only allows the main, undeviated electrons to pass through and form image at the screen. On the other hand, only one of the beams reflected from a particular plane is allowed by the aperture in the dark-field image. Dark-field imaging thus depends on the particular diffracted beam (particular *hkl* plane) selected.

JEOL JEM-2010 electron microscope in Fig. 2.17 is used to study the crystal structure of grown layers. It has a $LaB_6$ electron gun and can be operated between 80 and 200 kV with a point resolution of 0.23 nm.

Figure 2.17 Photo of the JEOL JEM-2010 electron microscope.

## 2.5 X-ray Diffraction (XRD) Technique

X-ray diffraction is a technique used to determine material structures and phases of a sample. In addition to structural and phase analysis, other application for XRD includes semi-quantitative phase analysis (Dickson et al., 1969), relative degree of crystallinity measurement (Zheng et al., 2000), particle analysis (Zhang et al., 2002), film thickness analysis (Stacy et al., 1974), and stress analysis (Kamigaki et al., 1986).

The operating principles of XRD can be explained by the Bragg's law. When a material (sample) is irradiated with a parallel beam of monochromatic X-rays, the X-

ray beams are diffracted to specific angles from the atomic lattice of the sample which acts as a 3D diffraction grating. Each detected X-ray signal from the diffraction pattern corresponds to coherent reflection, called a Bragg reflection, from successive planes of the sample for which Bragg's law is satisfied

$$2d\sin\theta = n\lambda \tag{2.2}$$

as shown in Fig. 2.17, where $d$ = atomic spacing between the planes

$\theta$ = angle that X-ray beam makes with respect to the plane

$\lambda$ = wavelength of the X-rays

$n$ = 1,2,3,........

For simple cubic crystal, the distance d between the crystallographic planes with indices *hkl* is

$$d = \frac{a}{\sqrt{h^2 + k^2 + l^2}} \tag{2.3}$$

In this work, XRD measurements are carried out using D8 (BRUKER) X-ray diffractometer shown in Fig. 2.18. It is used to determine the lattice constants of the $In_xGa_{1-x}As$ grown layers, In composition and the level of strain remained in the epilayers.

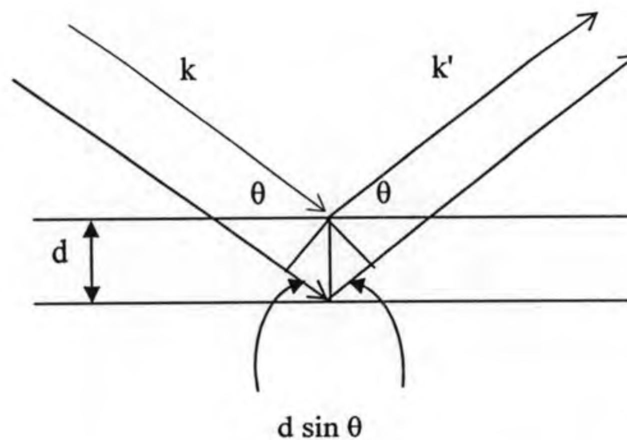


Figure 2.18 Reflection of X-ray beam incident at the angle θ off two parallel planes separated by the distance (d).

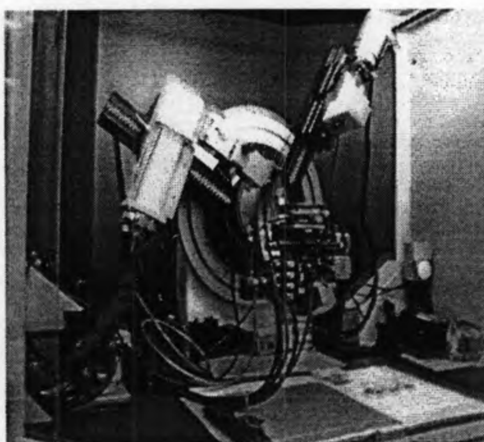

Figure 2.19 Photo of the (D8 BRUKER) X-ray Diffractometer System.

**Conclusion**

Important experimental techniques involved in this thesis which includes MBE growth and characterisation tools are explained in this chapter. For in-situ MBE growth characterisation, mass spectroscopy and RHEED are explained. For ex-situ characterisation tools, AFM, TEM, PL and HRXRD are explained. These techniques are useful for surface morphology (AFM), cross-section (TEM), optical (PL) and strain (XRD) properties and analyses.

Next chapter presents self-assembled nanostructure growth via three kinds of growth modes from experimental and theoretical points of view. In addition, defects and dislocations in strained semiconductor heterostructures are explained in order to understand the many aspects of semiconductor materials. Various ordered quantum dot growth techniques are reviewed for further optimized growth of ordered QDs.